Journal of Molecular Catalysis A: Chemical 321 (2010) 61–70

Contents lists available at ScienceDirect

Journal of Molecular Catalysis A: Chemical

journal homepage: www.elsevier.com/locate/molcata

# Cr-free Fe-based water-gas shift catalysts prepared through propylene oxide-assisted sol–gel technique

Preshit Gawade, Burcu Mirkelamoglu, Bing Tan, Umit S. Ozkan*

*Department of Chemical and Biomolecular Engineering, The Ohio State University, 140W. 19th Avenue, Columbus, OH 43210, United States*

ARTICLE INFO

*Article history:*
Received 27 November 2009
Received in revised form 24 January 2010
Accepted 1 February 2010
Available online 6 February 2010

*Keywords:*
Propylene oxide
Citric acid
Fe–Al–Cu
WGS
Maghemite
Formate
TPO
Copper
Sol–gel
Magnetite
XPS
DRIFTS

ABSTRACT

Chromium-free Fe-based water-gas shift catalysts were prepared through a gelation agent-assisted sol–gel route utilizing propylene oxide and citric acid as the gelation agents. Catalyst preparation using propylene oxide is a "one-pot" method that is cleaner, more eco-friendly and less time consuming over our previously developed sol–gel method for preparing Fe–Al–Cu and leads to comparable activities. The effect of Cu loading on the performance of Fe–Al–Cu catalyst was investigated using a syngas mixture as feed. The optimized Fe–Al–Cu formulation demonstrated stable WGS performance over a wide temperature range (250–400 °C). X-ray diffraction patterns revealed the role of promoters in the formation of maghemite phase and in controlling the crystallite size. The incorporation of copper in iron oxide matrix resulted in formation of maghemite phase over hematite, thereby causing a significant improvement in WGS performance. Diffuse reflectance infrared Fourier transform spectroscopy (DRIFTS) study of CO adsorption indicated the formation of formate species on the surface. The apparent activation energies for re-oxidation of the Fe–Al–Cu catalysts were found to depend on the copper content. Over the best performing Fe–Al–Cu catalyst, surface re-oxidation by water during WGS reaction proceeds at a much higher rate than surface reduction via CO oxidation, whereas for other catalysts of the series, surface re-oxidation was shown to be the rate determining step.



## 1. Introduction

The WGS reaction remains an important step in hydrogen production from syngas, especially in light of the increased emphasis on use of hydrogen for fuel cell applications. The syngas can be derived from steam reforming of natural gas or liquid hydrocarbons and coal/biomass/municipal waste gasification. The syngas composition depends upon various factors such as feedstock properties, operating conditions and reactor type. Typically, it is a mixture of CO, $CO_2$, $H_2$, $H_2O$, $CH_4$ and traces of higher hydrocarbons. The syngas may also contain trace quantities of $H_2S$ and COS depending on the feedstock. The effectiveness of gas cleaning processes further determines the final composition of the syngas. The currently available WGS units operate in a two-stage mode, namely, high-temperature WGS (HT-WGS) followed by low-temperature shift (LT-WGS) [1–3]. Commercially, HT-WGS is operated in the temperature range of 320–450 °C in the presence of Fe–Cr catalyst, whereas, LT-WGS operates in the range of 200–250 °C over $Cu/ZnO/Al_2O_3$ catalyst [2,4,5]. Both catalytic systems have been reviewed in many recent articles [6,7]. The two-stage operation mode is a consequence of several drawbacks of the current catalytic systems for WGS. HT-WGS catalyst, Fe–Cr, is not active at lower operating temperatures, while LT-WGS catalyst, $Cu/ZnO/Al_2O_3$, experiences severe sintering at higher temperatures. This necessitates the use of highly impractical and cost ineffective two-stage WGS units. In addition, the commercial Fe–Cr catalyst contains around 8–14 wt% of Cr, as a structural promoter as well as a stabilizer to prevent the particle sintering at elevated temperatures [8–10]. However, $Cr^{6+}$ is highly carcinogenic and environmentally unacceptable. Furthermore, these formulations demand high steam and experience considerable sulfur poisoning. Therefore, it is essential to develop a Cr-free catalytic system, which can be operated in a wide temperature range.

The sol–gel method for catalyst preparation method is considered to be more effective in terms of offering improved homogeneity, high purity, low calcination temperature and ability to tailor the desired metal oxide phase over traditional preparation methods [11,12]. The sol–gel method is basically a two-step process in which metal salt undergoes hydrolysis reaction followed by the condensation to form nano-scale structures. Formation of iron oxide matrix using sol–gel techniques in which the gel formation was induced by heating, adding a base or a gelation agent was reported (cited in [13]). In the past, several researchers synthesized nano-scale Fe as well as spinel oxides using epoxides such as

* Corresponding author. Tel.: +1 614 292 6623; fax: +1 614 292 3769.
*E-mail address:* ozkan.1@osu.edu (U.S. Ozkan).

1381-1169/$ – see front matter © 2010 Elsevier B.V. All rights reserved.
doi:10.1016/j.molcata.2010.02.002

ethylene oxide and propylene oxide [12–14]. These gelation agents were reported to provide high homogeneity, high purity and high surface area [12–14]. The ratio of epoxide to metal salt [13,14] as well as the choice of solvent play a critical role in gel formation rate and determining the particle size. The epoxides are believed to act as proton scavengers that cause iron to undergo hydrolysis and condensation processes to form an iron oxide matrix [13]. However, it is worthwhile to note that ethylene oxide is highly carcinogenic and toxic which defeats the purpose of environmentally benign catalyst preparation methods. Citric acid is also another gelation agent, which is widely studied for the preparation of highly dispersed mixed-oxides such as bismuth oxide, cerium-zirconium oxide and spinel oxides of cobalt [11,15–18].

In previous publications [19,20] we reported the development of a novel, Cr-free Fe–Al–Cu catalytic system for WGS that could be operated in a wide temperature range of 250–400 °C. The mentioned Fe–Al–Cu catalyst was prepared via a one-pot sol–gel route. This formulation showed significantly higher WGS performance than commercially available Fe–Cr. However, this sol–gel technique was tedious, time consuming and required critical pH adjustment. Several washing steps involved in the catalyst preparation process resulted in generation of large quantities of liquid waste. Therefore, it was required to develop an easier, more environmentally friendly and less time consuming catalyst preparation process.

In this paper, we report development of Cr-free Fe-based formulations using two gelation agents, namely citric acid and propylene oxide. The developed sol–gel preparation methods using these gelation agents are simpler, less time consuming and above all, environmentally benign. Propylene oxide based Fe–Al–Cu system demonstrated significant WGS performance which was comparable to the previously reported Fe–Al–Cu sol–gel combination [19,20]. This propylene oxide based gelation technique is a simple "one-pot" technique and requires neither catalyst washing nor critical pH adjustments. Copper is an essential promoter in the Fe-based catalysts [8,9,19,21], therefore, the effect of Cu loading for catalysts prepared by this technique has also been investigated. In addition to steady-state experiments for WGS activity evaluation, numerous catalyst characterization techniques such as X-ray diffraction (XRD), temperature-programmed reduction (TPR) and oxidation (TPO), X-ray photoelectron spectroscopy (XPS), diffuse reflectance infrared Fourier transform spectroscopy (DRIFTS) and Brunauer–Emmett–Teller method (BET) were implemented in order to evaluate the surface as well as bulk properties of the catalysts which could be correlated to their WGS performance.

## 2. Experimental

### 2.1. Catalyst preparation

Fe-based catalysts with Cu and Al employed as promoters were prepared through a sol–gel route using propylene oxide and citric acid as gelation agents. Aluminum nitrate [$Al(NO_3)_3{\cdot}9H_2O$] (crystals, Fisher), iron (III) nitrate nanohydrate [$Fe(NO_3)_3{\cdot}9H_2O$] ((98+%) ACS reagent, Sigma–Aldrich) and copper (III) nitrate trihydrate [$CuN_2O_6{\cdot}3H_2O$] (Fluka) were used as metal precursors in catalyst preparation.

For preparation of catalysts with the propylene oxide route, metal salt(s) in quantities to yield the desired atomic ratios of Fe, Al and Cu in the final catalyst were dissolved in ethanol at ambient temperature. Propylene oxide was added at once to this solution in excess quantities while continuously stirring the solution. The addition of propylene oxide resulted in rapid heat evolution accompanied by gel formation. The gel was kept at 50 °C for 4 h and then dried overnight at 110 °C in a convection oven. Dried samples were ground to a fine powder and calcined in air for 4 h at 450 °C (heating rate: 10 °C/min). The samples were crushed to a fine powder following calcination. The propylene oxide method was utilized for preparation of Fe-only, Fe–Cu bi-metallic and Fe–Al–Cu ternary samples. The atomic ratio of Fe to Cu in Fe–Cu bi-metallic catalyst was 5, whereas Fe to Cu ratio was varied in Fe–Al–Cu catalysts (Fe/Cu = 10, 5 and 2) while keeping Fe/Al = 10 constant.

Another gelation agent that was utilized for the preparation of Fe-based WGS catalysts was citric acid. For the preparation of catalyst sample through the citric acid route, metal salts to yield the desired atomic ratios of the metals and citric acid were dissolved in a 1:1 (w/w) solution of ethanol and water at ambient temperature while stirring continuously. The ratio of moles of citric acid to the moles of total nitrate ($NO_3$) contained in the metal salts was kept constant at 1. The solution was kept at 80 °C for 3 h to slowly drive off ethanol and then dried in a convection oven overnight at 110 °C. The sample was then calcined in air at 450 °C (heating rate: 10 °C/min) for 4 h. The sample was ground to a fine powder following calcination.

### 2.2. Catalytic activity testing

All the steady-state experiments were conducted in a fixed-bed flow reactor system using 0.25″ OD stainless steel reactor. Catalyst samples were held in place by the stainless steel frit and a quartz wool plug and the temperature of the reactor bed was measured by an Omega K-type thermocouple. The reactor was placed inside a home-made, resistively heated furnace, the temperature of which was controlled by an Omega (model CS232) PID temperature controller. Reagent gases were supplied from Praxair and were used without any further treatment. Independent gas mass flow controllers (Brooks, 5850E) connected to an electronics control box (Brooks, 0154) were used to control gas flows to the system. Water vapor was supplied to the system by bubbling nitrogen through a heated bubbler containing de-ionized water. The temperature of the bubbler was monitored and controlled precisely by a temperature controller. Gas lines in contact with water vapor containing stream were heated using heating tapes in order to avoid water condensation in the lines.

Unless otherwise stated, 100 mg of catalyst sample was used for each run and the experiments were carried out at a WHSV (weight hourly space velocity) of 0.06 $m^3$ (g cat.)$^{-1}$ $h^{-1}$. In addition, steady-state experiments were conducted on equal surface area to ensure that the observed differences were not simply due to differences in surface areas. In order to assure that the activity testing experiments were run in the kinetically controlled regime, reaction conditions were maintained away from equilibrium in all of the activity testing experiments.

Prior to catalytic activity testing, catalyst samples were pretreated *in situ* in $N_2$ (67.5 sccm) for 30 min at 350 °C and then reduced at 350 °C for 2 h in syngas mixture (10% CO, 10% (or 20%) $H_2O$, 7.5% $H_2$, 5% $CO_2$ balanced with 67.5% $N_2$). Finally, reaction studies were performed over the wide temperature range (250–400 °C) in the above mentioned syngas mixture.

The feed as well as the reactor effluents were analyzed by an online gas chromatograph (Shimadzu, GC-14A series) equipped with a thermal conductivity detector (TCD). Argon was used as the carrier gas and the gas separation was performed using a molecular sieve column 13X (5 ft × 1/8 in. SS, 60/80 mesh) and a porapak Q column (12 ft × 1/8 in. SS, 80/100 mesh).

### 2.3. Catalyst characterization

#### 2.3.1. Specific surface area and pore volume

The specific surface areas of the samples were measured on Micromeritics ASAP 2010 surface area analyzer using $N_2$ physisorption technique. Prior to analysis, samples were degassed overnight at 130 °C under a vacuum of 3 μm Hg. The specific surface areas

were determined by the Brunauer–Emmett–Teller (BET) method using the adsorption branch of the isotherm. Pore volumes of the samples were determined by the Barrett–Joiner–Halenda (BJH) method using the adsorption branches of the $N_2$ physisorption isotherms.

*2.3.2. X-ray diffraction*

X-ray diffraction (XRD) patterns of the pristine samples were collected on a Rigaku X-ray diffractometer (X-ray source: Cu Kα radiation, λ = 1.5418 Å) operated at 40 kV and 25 mA. The diffraction patterns were collected in the range of 20–60° Bragg angle values. The X-ray diffraction patterns of the reduced catalyst samples were collected on a Bruker D8 Advance X-ray diffractometer equipped with a capillary sample holder. Following reduction treatment, the samples were transferred to an Ar-purged glove box that contains minimal residual air (<5 ppm). The samples were transferred to capillary sample tubes (0.2 mm OD) and the ends of the capillary tube were sealed inside the glove box with glass sealant. The samples were then transferred air-free to capillary sample holder accessory on the diffractometer. The diffraction patterns were collected in the 20–70° Bragg angle range using a Cu Kα X-ray source (λ = 1.5418 Å) operated at 40 kV and 50 mA.

*2.3.3. X-ray photoelectron spectroscopy*

X-ray photoelectron spectroscopy was used for the investigation of the chemical states of copper and iron in the calcined (pristine) and reduced samples. The samples referred to as 'pristine' were ground into double sided carbon tape directly following calcination and transferred to the vacuum chamber of the XPS instrument. The reaction system described in Section 2.2 was used for preparing the pretreated samples. The 'reduced' samples were prepared through treatment in syngas mixture containing 10% CO, 10% $H_2O$, 7.5% $H_2$ and 5% $CO_2$ in $N_2$ (100 sccm) at 350 °C for 2 h. Following pretreatment, the reactor was flushed with $N_2$ for 30 min at 350 °C and the reactors were allowed to cool down to room temperature under $N_2$ flow before sealing under $N_2$. The sealed reactors were transferred to a glove box kept under Ar atmosphere with moisture content lower than 5 ppm. The samples were ground into a carbon tape inside the glove box and then transferred air-free to the vacuum chamber of the XPS instrument. The X-ray photoelectron spectra were collected on a Kratos Axis Ultra spectrometer using Kα radiation through Al anode operated at 13 kV and 10 mA. When necessary, the charge neutralizer was operated at a current of 2.1 A and a filament bias of 1.3 V. Concurrent sweeps of Cu 2p, Fe 2p, O 1s and C 1s envelopes were collected. The collected spectra were corrected using C 1s envelope located at 284.5 eV. For comparability of the signal intensities of the envelopes, counts per second, were divided by the number of sweeps and the transmission value at the specific binding energy. Background correction and peak fitting were done using the XPSPeak 4.1 software.

*2.3.4. Diffuse reflectance infrared Fourier transform spectroscopy*

The adsorption and thermal transformations of CO on Fe–Al–Cu based catalysts was investigated using an FT-IR spectrometer (Thermo Nicolet 6700) equipped with an MCT detector and a DRIFTS chamber with ZnSe windows. The DRIFT spectra were collected in the mid-IR range at a nominal resolution of 4 $cm^{-1}$ and the final spectra were averaged over 500 scans. For each experiment, catalyst sample was reduced in syngas mixture in a reactor system at 350 °C for 2 h as mentioned in Section 2.1. The reduced catalysts were recovered under $N_2$ atmosphere and transferred to DRIFTS cell to acquire spectra. The sample was pretreated in He (30 sccm) at 400 °C for 30 min, followed by background spectra collection in He (30 sccm) from 400 °C to room temperature while cooling down the sample. Helium was switched off after background collection and system was flushed with CO (30 sccm) for 30 min at room temperature. Catalyst temperature was raised under the flow of CO (30 sccm) from room temperature to 400 °C stepwise and spectra were collected at regular temperature intervals.

*2.3.5. Transmission electron microscopy*

Transmission electron microscopy (TEM) was carried out using Phillips Tecnai F20 instrument with FEG operated at a voltage of 200 kV. The catalyst images were collected in brightfield mode. Catalyst sample was dispersed in ethanol and the mixture was sonicated for 20 min. The sample was then deposited onto 200 mesh copper grid coated with lacey carbon.

*2.3.6. Temperature-programmed characterization*

Temperature-programmed reduction (TPR) and temperature-programmed re-oxidation experiments were conducted in order to provide insights to the oxidation/reduction characteristics of the samples. For the temperature-programmed reduction experiments, 50 mg of calcined catalyst sample was packed in a 0.25″ OD U-tube quartz reactor. Catalyst was pretreated in He (35 sccm) at 350 °C for 30 min and then cooled down to room temperature under the same atmosphere. Finally, temperature of the catalyst bed was raised to 880 °C at 10 °C/min under the flow of the reducing agent, 5%$H_2$/$N_2$ (20 sccm). Hydrogen consumption during the temperature ramp was monitored by a thermal conductivity detector (TCD).

For the temperature-programmed re-oxidation experiments, 100 mg of sample was packed in a fixed-bed quartz reactor with a quartz frit bed which is placed inside a fast response furnace (Carbolite, MTF 10/15/130). The dead volume of the reactor was filled with quartz wool. The reactor effluents during pretreatment and temperature-programmed re-oxidation stages were monitored via a residual gas analyzer (MKS-Cirrus II) operated in scanning ion mode. An electron multiplier detector was used to trace mass signals ($m/z$) 2, 16, 18, 32 and 44. The gas lines from the reactor to the mass spectrometer capillary inlet were heated via a heating cord to prevent condensation during pretreatment and the experiment. Each experiment consisted of a reduction stage where the sample was heated at 10 °C/min to 300 °C under He atmosphere and then, reduced with 5%$H_2$/He (40 sccm) at the same temperature for an hour. Reduction was followed by He flush (40 sccm) at 300 °C prior to cooling to room temperature under helium. Once the sample was at room temperature, 5% $O_2$/He (40 sccm) introduced to the reactor. The mass traces on the mass spectrometer were allowed to stabilize at room temperature and then, a linear temperature program from 30 to 450 °C was enacted with isothermal stages lasting for 20 min at 30 and 450 °C. The same temperature-programmed re-oxidation experiment was repeated with different heating rates for the determination of activation energies of re-oxidation of Fe–Al–Cu samples. The samples were treated following the same pretreatment procedure and heated at 10, 14 or 18 °C/min during the temperature-programmed re-oxidation stage. Kissinger's method [22] was used for estimating the activation energies of re-oxidation. Kissinger's method correlates the temperature at which the maximum rate of oxidant consumption occurs with the activation energy for re-oxidation through a series of temperature-programmed experiments ran at different heating rates. The temperature at which the maximum rate of oxidant consumption occurs corresponds to the sample temperature at which the deflection of the oxidant consumption peak takes place ($T_m$). The activation energy can be estimated through a plot of $1/T_m$ versus $\ln(\Phi/T_m^2)$ which yields a straight line with the slope being equal to $-E_a/R$, where $\Phi$ is the heating rate in K/min; $-E_a$ is the activation energy in J/mol; and $R$ is the universal gas constant in J/K mol.

## 3. Results and discussion

### 3.1. Effect of gelation agent on WGS activity

In our previous publications, we have reported the development of Cr-free Fe–Al–Cu catalyst formulations which exhibited superior WGS performance over the commercial Fe–Cr catalyst in a wide temperature range [19,20]. We also showed that the preparation method played a key role on the WGS performance of these catalysts. Our initial work involved catalyst preparation through co-precipitation of Fe and Al from nitrate precursors followed by impregnation of Cu onto the calcined precipitate (two-step) and co-precipitation of Fe–Al–Cu using nitrate precursors and sodium carbonate as the precipitating agent (one-step) [23]. In a later publication, we reported catalyst development through a 'one-pot' sol–gel-precipitation route using organic precursors [19]. The Fe–Al–Cu samples prepared through this sol–gel/precipitation route showed significant enhancement in the WGS activity compared to the two-step and one-step routes. However, this sol–gel/precipitation method required critical pH adjustment, which was achieved through addition of NaOH and involved extensive catalyst washing to remove the sodium ions afterwards.

To address the issues associated with catalyst preparation, we have investigated the applicability of a gelation agent-assisted sol–gel 'one-pot' route using propylene oxide as the gelation agent. Fe-only, Fe–Cu and Fe–Al–Cu samples were prepared by the propylene oxide-assisted sol–gel route. The monometallic Fe catalyst prepared by propylene oxide-assisted sol–gel route exhibited a reasonable CO conversion of 30% at 400 °C in a syngas mixture. The textural promoter (Al) and structural promoter (Cu) were incorporated in the catalysts in order to improve their WGS activity. Al and Cu have been reported to be effective promoters [3,8–10,19–21]. Among the promotional effects that are reported are structural and textural promotion, which include improved surface area, resistance to sintering and change in the electronic properties of the magnetite phase. As expected, further improvement was achieved in the WGS activity by incorporation of Cu and Al in the catalysts prepared by propylene oxides-assisted sol gel technique, achieving CO conversions of 40% and 57% over Fe–Cu (Fe/Cu = 5) and Fe–Al–Cu (Fe/Al = 10 and Fe/Cu = 5), respectively. The equilibrium CO conversion under these conditions is 64%.

Similar Fe-based water-gas shift catalysts were also prepared by using another commonly used gelation agent, citric acid, and tested with regards to their activity in the syngas mixture. The Fe-only catalyst prepared through the citric acid route showed slightly higher WGS activity than the Fe-only catalyst prepared through the propylene oxide route however, the activity was not stable with time-on-stream. Further investigation of the WGS activity of Fe–Al–Cu (Fe/Al = 10 and Fe/Cu = 5) catalyst prepared through the citric acid route showed that, the activity of this catalyst was not stable either and the initial CO conversion of 40% over this catalyst decreased to less than 20% with time-on-stream over a period of 10 h. Although the citric acid-assisted route was shown to be unsuitable for preparation of active and stable Fe–Al–Cu catalysts, the initial catalyst testing results showed that it was possible to prepare active and stable Fe–Al–Cu catalysts through the propylene oxide-assisted sol–gel route. Therefore, the structural properties of Fe-based catalysts prepared through the propylene oxide route and the effect of copper loading on their performance was further investigated.

### 3.2. Effect of Cu loading on the WGS activity

Sol–gel Fe-based catalysts with different Cu loadings (Fe/Cu = 10, 5 and 2) and constant aluminum loadings (Fe/Al = 10) were prepared using the propylene oxide-assisted route in order to investigate the effect of copper loading on the WGS activity of these catalysts and to elucidate the structural changes induced by copper incorporation. Table 1 presents the specific surface areas and pore volumes of these Fe–Al–Cu catalysts. The surface area was found to be strongly dependent on copper loading and it decreased with increasing Cu content of the catalysts. A similar trend was observed in pore volume. As it will be discussed in the following sections, incorporation of copper in Fe-based catalysts resulted in significant changes in the catalyst structure, especially in the major crystalline phases and particle size, as well as catalytic performance.

**Table 1**
BET surface area, and pore volume of Fe–Al–Cu catalysts at various Cu loadings.

| Catalyst | BET surface area ($m^2/g$) | BJH adsorption pore volume ($cm^3/g$) |
|---|---|---|
| Fe/Cu = 10 | 99 | 0.1830 |
| Fe/Cu = 5 | 46 | 0.1669 |
| Fe/Cu = 2 | 25 | 0.0421 |

#### 3.2.1. Catalytic activity testing

Fig. 1a shows the WGS activity of the three Fe–Al–Cu samples a wide temperature range (250–400 °C) in syngas mixture at WHSV of 0.06 $m^3$ (g cat.)$^{-1}$ $h^{-1}$ at a steam-to-carbon (S/C) feed ratio of 1. WGS activity was significantly improved when Cu content was increased from Fe/Cu = 10 to Fe/Cu = 5. The Fe–Al–Cu (Fe/Cu = 5) sample was able to achieve CO conversion in excess of 55% in a broad temperature window of 300–400 °C. The equilibrium CO conversion at 400 °C under these reaction conditions was 64%. However, Fe–Al–Cu (Fe/Cu = 10) sample was able to achieve a maximum CO conversion of slightly lower than 40%. Further increase in Cu content affected WGS activity adversely, resulting in considerable drop in CO conversion. This catalyst was able to achieve only 27% CO conversion in 300–400 °C. A similar effect of copper content on the WGS activity of copper-doped magnetite catalysts was also reported by Quadro et al. [8]. When a commercial Fe–Cr catalyst was tested under identical conditions, the CO conversions achieved were much lower, even when compared to the least active of the formulations tested, i.e., Fe–Al–Cu (Fe/Cu = 2).

Since the catalysts with different Cu loadings were compared at equal WHSV, a valid question would be if the differences in activities could be due to the differences in surface areas. To address this question, WGS activity of Fe–Al–Cu (Fe/Cu = 2) and Fe–Al–Cu (Fe/Cu = 5) samples were also tested on an equal BET surface area basis. The reactions were carried out at 400 °C with the same reaction feed as the above mentioned activity tests. The Fe–Al–Cu (Fe/Cu = 2) sample was found to exhibit significantly lower CO conversion than Fe–Al–Cu (Fe/Cu = 5). The CO conversion over Fe–Al–Cu (Fe/Cu = 2) sample was 30%, whereas it was 41% over Fe–Al–Cu (Fe/Cu = 5) at 400 °C on equal surface area basis. Therefore, decrease in CO conversion over Fe–Al–Cu (Fe/Cu = 2) cannot be explained with the decrease in surface area.

The Fe–Al–Cu (Fe/Cu = 5) catalyst was further tested for stability. The inset to Fig. 1a shows CO conversion over this catalyst during WGS in syngas mixture as a function of time-on-stream at 400 °C. The catalyst was observed to exhibit stable WGS activity with time-on-stream over a period of 40 h.

The WGS activity of the Fe–Al–Cu catalysts was further investigated at a higher steam-to-carbon ratio of the reaction feed. Fig. 1b shows the CO conversions achieved as a function of temperature over Fe–Al–Cu catalysts during WGS reaction at a steam-to-carbon ratio of 2. At low temperatures no significant effect of increasing steam-to-carbon ratio on the WGS activity was observed; however, at higher temperatures, increased steam content of the feed resulted in a significant increase in CO conversion. Although an increase in the stream content resulted

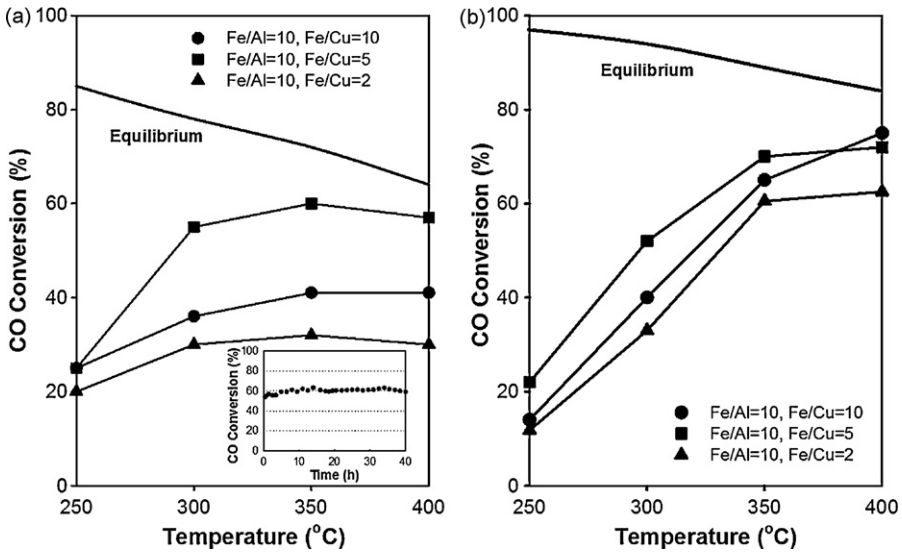


**Fig. 1.** WGS activity (CO% conversion) of Fe–Al–Cu catalysts prepared by propylene oxide-assisted sol–gel method with different Cu loadings at (a) S/C = 1 and (b) S/C = 2. Inset: time-on-stream performance of Fe–Al–Cu (Fe/Cu = 5) at 400 °C at S/C = 1. *Reaction conditions*: [CO] = 10%, [$H_2O$] = 10% or 20%, [$CO_2$] = 5%, [$H_2$] = 7.5% and balance $N_2$, WHSV = 0.06 $m^3$ (g cat.)$^{-1}$ $h^{-1}$, $P$ = 1 atm.

in a shift in CO conversion curves to higher values over all of the samples by accelerating the forward reaction, it had a more pronounced effect over Fe–Al–Cu (Fe/Cu = 10) and Fe–Al–Cu (Fe/Cu = 2) than Fe–Al–Cu (Fe/Cu = 5). At 400 °C, the CO conversion over Fe–Al–Cu (Fe/Cu = 5) increased from 57% to 72% with increasing steam-to-carbon ratio, whereas the CO conversion over Fe–Al–Cu (Fe/Cu = 10) and Fe–Al–Cu (Fe/Cu = 2) almost doubled. As it will be discussed in Section 3.2.5, the re-oxidation of Fe–Al–Cu (Fe/Cu = 10) and Fe–Al–Cu (Fe/Cu = 2) is expected to proceed at a much slower rate than the re-oxidation of Fe–Al–Cu (Fe/Cu = 5) during reaction. The fact that Fe–Al–Cu (Fe/Cu = 10) and Fe–Al–Cu (Fe/Cu = 2) catalysts benefit more from the increased steam content of the feed as compared to Fe–Al–Cu (Fe/Cu = 5) implies that the re-oxidation of surface through water splitting during WGS reaction is the rate limiting step over these catalysts under these conditions.

### 3.2.2. X-ray diffraction

X-ray diffraction was used to examine the effect of copper incorporation and copper loading on the crystal phases formed during catalyst preparation. The X-ray diffraction pattern of the Fe-only sample showed the presence of α-$Fe_2O_3$ (hematite) phase, as evidenced by diffraction features located at Bragg angle (2$\theta$) values of at 24.2°, 33.2°, 35.7°, 40.9° and 49.5° (Fig. 2a) which can be associated with (0 1 2), (1 0 4), (1 1 0), (1 1 3) and (0 2 4) crystal planes, respectively. Hematite phase disappeared with the incorporation of Cu into the iron oxide matrix. The X-ray diffraction pattern of Fe–Cu (Fe/Cu = 5) reflected the formation of γ-$Fe_2O_3$ (maghemite) phase instead of hematite phase. The diffraction lines at Bragg angle (2$\theta$) values of 30.1°, 35.6° and 43.2° (Fig. 2b) were associated with (2 2 0), (3 1 1) and (4 0 0) planes of maghemite, respectively. This maghemite phase was retained even after the addition of Al (Fig. 2c–e). Maghemite is considered to be more active than hematite phase for WGS [10]. In addition, maghemite phase is in an imperfect cubic spinel structure, which is similar to the WGS active phase, $Fe_3O_4$ (magnetite) [1,2,10,24]. This imperfect structure of maghemite allows better incorporation of active promoters than hexagonal hematite phase. Consequently, active promoter incorporated in maghemite is less prone to sintering effects [10,25]. Also Fig. 2a–c showed that the addition of promoters lead to broadening of diffraction lines which could be correlated to a decrease in the crystallite size.

The X-ray diffraction patterns of Fe–Al–Cu (Fe/Cu = 10) and Fe–Al–Cu (Fe/Cu = 5) samples (Fig. 2c and d, respectively) showed diffraction lines located at 2$\theta$ values of 30.1°, 35.6° and 43.2° which can be associated with (2 2 0), (3 1 1) and (4 0 0) planes of maghemite. No other phases that could be related to the presence of copper in the structure were detected in either of the samples. Unlike these two catalysts, the sample with the highest amount of copper loading (Fe/Cu = 2) consisted of peaks that could be associated with maghemite as well as a separate CuO phase, which was identified through peaks located at 38.6° and 48.6°. The development of a separate CuO phase in the Fe–Al–Cu (Fe/Cu = 2) sample but not in Fe–Al–Cu (Fe/Cu = 5) suggests that there is a certain amount of copper atoms that could be incorporated into the iron oxide matrix. We have previously observed the separation of cop-

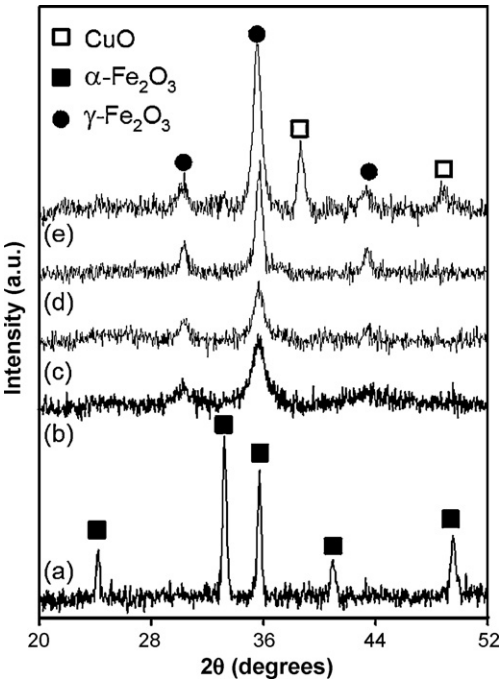


**Fig. 2.** XRD patterns of Fe-based samples. (a) Fe-only, (b) Fe–Cu (Fe/Cu = 5), (c) Fe–Al–Cu (Fe/Cu = 10), (d) Fe–Al–Cu (Fe/Cu = 5) and (e) Fe–Al–Cu (Fe/Cu = 2).

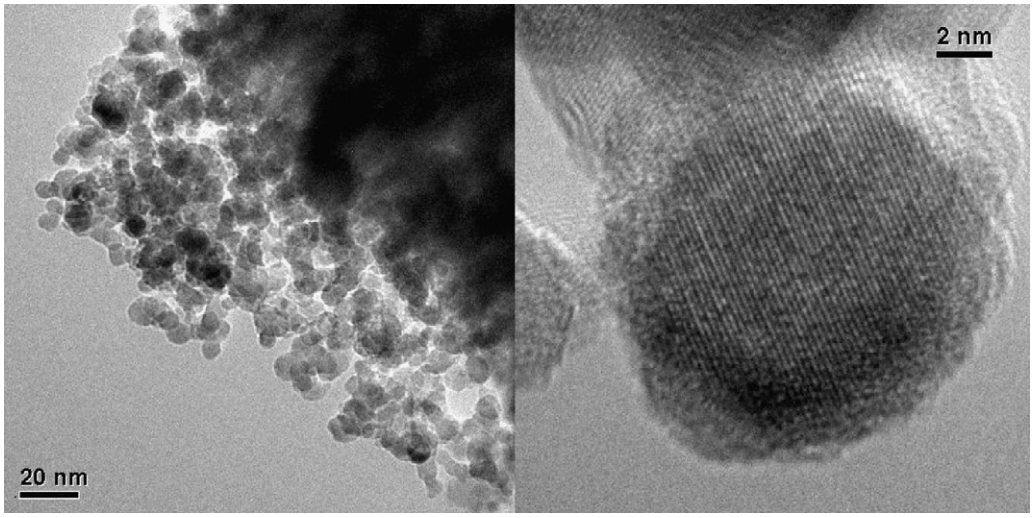


**Fig. 3.** Transmission electron micrographs (TEM) of Fe–Al–Cu (Fe/Cu = 5).

per in the form of CuO domains on Fe–Al–Cu samples prepared through the sol–gel route and suggested that there was a limit on the amount of copper atoms that could be incorporated into the iron oxide matrix [20]. We have further suggested that the amount of copper that could be incorporated into the iron oxide matrix lied in between Fe/Cu = 5 and 2, with the latter being an upper limit for Cu incorporation. Fe–Al–Cu samples prepared through the propylene oxide-assisted sol–gel route described in this study showed similar behavior, also suggesting that the maximum amount of copper that could be incorporated in the iron oxide matrix is a function of the charge structure of the system, rather than being dependent on the catalyst preparation route. Cu is an active promoter and modifies electronic properties of iron catalyst [5,19,20,26] as long as it is incorporated in the iron oxide matrix. The optimum amount of Cu in iron oxide matrix facilitates the formation of WGS active maghemite phase and improves surface area of Fe-based catalysts, as shown earlier. However, metallic Cu on the surface is more prone to sintering at high operating temperatures [19,20] which can result in poor WGS activity. The catalytic activity results presented in Section 3.2.1 are in agreement with these findings.

The crystallite size in Fe–Al–Cu samples was calculated through the Scherrer equation. The crystallite size of Fe–Al–Cu samples increased with increasing copper loading (Table 2) indicating the formation of larger, ordered crystals with the incorporation of increasing amounts of copper into the structure. The formation of crystals with longer range order was also evidenced with the decrease in the specific surface area of the samples with increasing copper loading. The crystallite size calculations were in line with transmission electron microscopy (TEM) images, which show the presence of uniform, nano-sized (~12 nm) particles of Fe–Al–Cu sample, as shown in Fig. 3. The lattice fringes for (4 0 0) plane of maghemite with a *d*-spacing of 1.70 Å is visible in the TEM image of Fe–Al–Cu (Fe/Al = 10, Fe/Cu = 5) catalyst.

The capillary XRD technique was used to study the reduced Fe–Al–Cu samples in order to avoid oxidation of the catalyst surface during the sample transfer. The reduced samples were pretreated in nitrogen and then reduced in syngas mixture (refer to Section 2.2). Fig. 4 shows XRD patterns of the reduced samples of Fe–Al–Cu at different Cu loadings. Magnetite phase (resulting from reduction of maghemite) was observed through peaks associated with (2 2 0), (3 1 1), (4 0 0), (5 1 1) and (4 4 0) planes at Bragg angle ($2\theta$) values of 30.1°, 35.4°, 43.3°, 57.4°, and 62.7°, respectively, in Fe–Al–Cu (Fe/Cu = 10) and Fe–Al–Cu (Fe/Cu = 5) samples. The XRD pattern of Fe–Al–Cu (Fe/Cu = 2) sample, along with magnetite phase, also contained intense peaks of metallic copper ($Cu^0$) at 43.2° and 50.3° which correspond to diffraction from (1 1 1) and (2 0 0) planes.

**Table 2**
Crystallite size of Fe–Al–Cu catalysts at various Cu loadings calculated from the XRD patterns through Scherrer equation.

| Catalyst | Crystallite size (nm)* |
|---|---|
| Fe/Cu = 10 | 11 |
| Fe/Cu = 5 | 12 |
| Fe/Cu = 2 | 15 |

* Crystal size calculated using Scherrer equation.

### 3.2.3. X-ray photoelectron spectroscopy

X-ray photoelectron spectroscopy was used to investigate the chemical states of iron and copper over the pristine samples and the changes that take place during catalyst activation via reduction in syngas. Fig. 5 shows the Cu 2p envelopes of pristine and reduced samples of Fe–Al–Cu catalysts with Fe/Cu ratios of 10, 5 and 2. In order to prevent interaction of the reduced samples with ambient air, the reduced samples were transferred air-free from the reactor to the vacuum chamber of the XPS instrument under an inert atmosphere.

The Cu 2p envelopes of the pristine samples resembled each other regardless of the copper content of the catalyst. Fig. 5 also shows the curve fitting for identification of photopeaks. In all of the

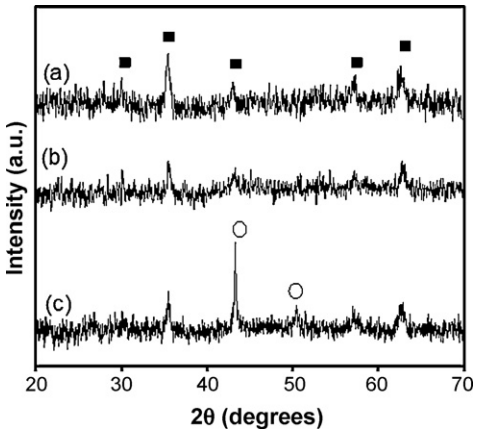


**Fig. 4.** XRD patterns of Fe–Al–Cu samples reduced in syngas mixture: (a) Fe/Cu = 10, (b) Fe/Cu = 5 and (c) Fe/Cu = 2.

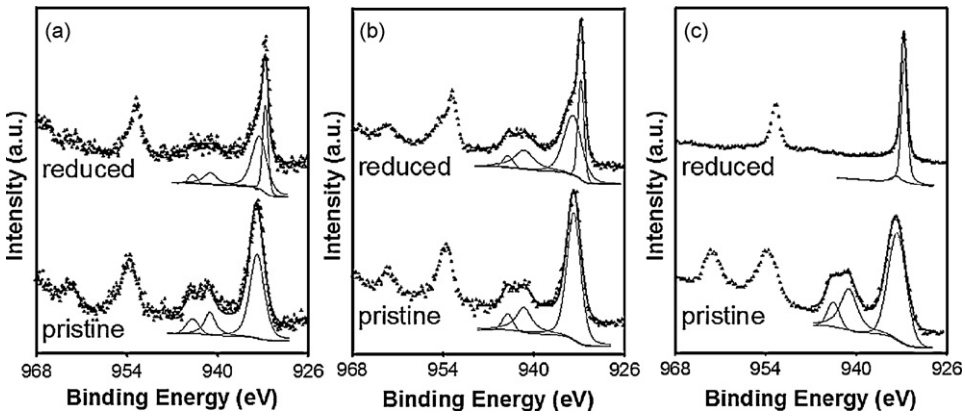


**Fig. 5.** X-ray photoelectron spectra of Cu 2p region of pristine and reduced Fe–Al–Cu samples: (a) Fe/Cu = 10, (b) Fe/Cu = 5 and (c) Fe/Cu = 2.

samples, the Cu $2p_{3/2}$ component of Cu 2p envelope was located at 933.3 eV with shake-up satellite lines at 941.0 eV ($\Delta E_B$ = 7.7 eV) and 943.1 eV ($\Delta E_B$ = 9.8 eV). The spin orbit splitting (SOS) of Cu $2p_{3/2}$ and Cu $2p_{1/2}$ was 19.8 eV, and the satellite peak for $2p_{1/2}$ was located at 961.7 eV ($\Delta E_B$ = 8.6 eV). The appearance of shake-up satellite peaks is common for paramagnetic species and the observed displacement in these together with the position of the photoelectron lines in the Cu 2p region suggests the presence of $Cu^{2+}$ ions in CuO environment as the major component [27,28].

Following reduction treatment, lower oxidation state copper species were observed together with cupric oxide over all of the samples. It is well known that reduction of copper oxide occurs during irradiation with the X-ray beam in the XPS instrument [29,30] and it is worthwhile to note that, we have observed the presence of $Cu^{2+}$ over pristine samples under similar experimental conditions and irradiation periods in the XPS instrument as the sole copper species. It is plausible that interaction of copper species with iron oxide network leads to increased stability of the CuO species over Fe–Al–Cu samples compared to pure cupric oxide. In line with the above discussion, the presence of copper species with lower oxidation states over the reduced samples is likely to be associated with the preceding treatment steps rather than reduction during X-ray irradiation.

Curve fitting of Cu $2p_{3/2}$ region of the reduced samples suggested the presence of two components – located at 933.3 and 932 eV – contributing to this photopeak in all of the reduced samples. Over Fe–Al–Cu (Fe/Cu = 5) and Fe–Al–Cu (Fe/Cu = 10) catalysts, the shake-up lines that were displaced by 7.8 and 9.8 eV with respect to 2p3/2 were also observed. The higher binding energy component together with the shake-up lines was associated with $Cu^{2+}$ ions whose appearance have been attributed to stabilization through interaction with iron oxide matrix. The location of the lower binding energy component is characteristic of copper species at lower oxidation state, however differentiation of $Cu^{1+}$ and $Cu^0$ by the photoelectron lines is not possible as the difference in the core level binding energies of copper atoms in these environments is well within experimental uncertainty. Over Fe–Al–Cu (Fe/Cu = 2) the Cu 2p envelope was dominated by lower oxidation state copper species (i.e. $Cu^{1+}$ or $Cu^0$) with little contribution from a higher binding energy component. Although the binding energy difference between metallic copper and $Cu^{1+}$ ions in $Cu_2O$ environment is too low to allow spectral differentiation of these species, complementary evidence from the X-ray diffraction patterns presented in Section 3.2.2 allows to associate this photopeak with the presence of metallic copper on reduced Fe–Al–Cu (Fe/Cu = 2). The relative contributions of CuO and the lower oxidation state component of the Cu 2p envelope were calculated using the areas under the fitted components. The relative contribution from $Cu^{2+}$ to the Cu 2p envelopes of reduced Fe–Al–Cu (Fe/Cu = 10), Fe–Al–Cu (Fe/Cu = 5) and Fe–Al–Cu (Fe/Cu = 2) was 72%, 74% and 18%, respectively. The presence of higher amount of lower oxidation state components over Fe–Al–Cu (Fe/Cu = 2) in comparison to Fe–Al–Cu (Fe/Cu = 5) and Fe–Al–Cu (Fe/Cu = 10), can be attributed to the copper species which have not been incorporated into the iron oxide matrix over this catalyst. Deprived of the stabilizing effect of iron oxide matrix, this free CuO phase is more prone to reduction and sintering at elevated temperatures and harsher reducing conditions.

Fig. 6 shows the X-ray photoelectron spectra in the Fe 2p region of pristine and reduced Fe–Al–Cu samples with the three different Fe/Cu ratios of 2, 5 and 10. The X-ray photoelectron spectra of the pristine samples were similar and contributions of four different photopeaks were resolved. The photopeak located at 711.1 eV is

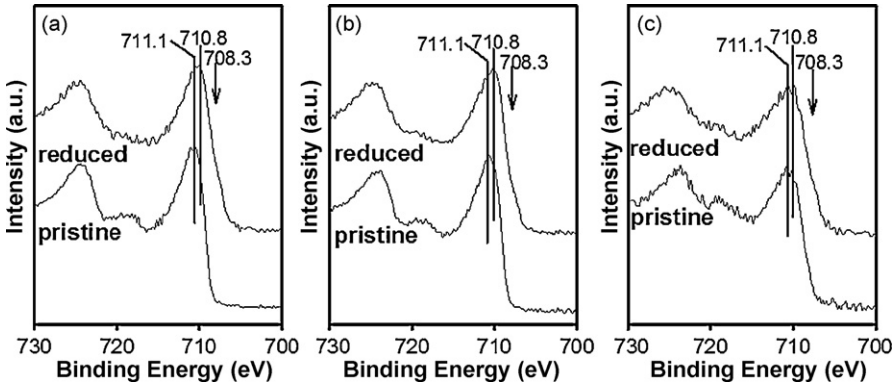


**Fig. 6.** X-ray photoelectron spectra of Fe 2p region of pristine and reduced Fe–Al–Cu samples: (a) Fe/Cu = 10, (b) Fe/Cu = 5 and (c) Fe/Cu = 2.

characteristic of core level Fe $2p_{3/2}$ photoelectrons of ferric oxide. The $2p_{3/2}$–$2p_{1/2}$ spin orbit splitting was 13.5 eV. The high degree of multiplet splitting of the Fe 2p core line resulted in the broad photopeaks observed in this region. Also observed were the satellite lines which were displaced by 8 eV. These satellite peaks were characteristic of $Fe_2O_3$. These satellite peaks are commonly used as fingerprints for different oxides of iron as the intensity and the position of the satellite peak is dependent on the environment of the $Fe^{3+}$ ions. However, $Fe^{3+}$ satellites were not the only photoelectrons that have contributions in this region in the case of Fe–Al–Cu samples. Since monochromatic Al Kα radiation which resulted in higher spectral resolution was used for obtaining well defined peak shapes, this region had contribution from Cu LMM Auger electrons at ca. 719 eV. The core level Fe 2p spectra of $Fe^{3+}$ species in α-$Fe_2O_3$ and γ-$Fe_2O_3$ environments are almost identical to each other. McIntyre and Zetaruk [31] used multiplet splitting patterns of Fe 2p core levels for identification of different oxides of iron. Through curve fitting of the Fe $2p_{3/2}$ peak these authors showed that the splitting of the two most intense components of the envelope was 1 eV for γ-$Fe_2O_3$ which was 0.2 eV lower than α-$Fe_2O_3$. In line with their findings, the curve fitting of the Fe 2p core level spectra of the pristine Fe–Al–Cu samples using the same parameters that these authors have used yielded a displacement of 1 eV between the two most intense components (not shown). Although more indirect than XRD, X-ray photoelectron spectroscopy provides complementary evidence for the presence of iron in the form of γ-$Fe_2O_3$ in the pristine samples. Following reduction treatment, the Fe 2p envelopes of all of the samples were similar to each other; the Fe $2p_{3/2}$ photopeak was located at 710.8 eV (SOS = 13.5 eV) with a weakly resolved shoulder that was displaced by 2.5 eV towards the lower binding energy side (Fig. 6). Another important feature of the Fe 2p envelope of the reduced samples was the disappearance of the shake-up lines, further indicated the transformation of $Fe_2O_3$ to $Fe_3O_4$ during reduction treatment. The X-ray photoelectron spectra suggested the presence of magnetite as the major phase and that the adopted reduction procedure resulted in partial reduction of iron as the presence of metallic iron (ca. 707 eV) was not detected in any of the samples.

### 3.2.4. Temperature-programmed reduction

The effect of copper loading on the reduction characteristics of Fe–Al–Cu samples was investigated with temperature-programmed reduction (TPR) in 80–880 °C region. Fig. 7 shows the $H_2$ consumption traces from these experiments. All of the samples exhibited a well-resolved consumption feature in 170–400 °C region and another broad consumption band that corresponded to higher temperatures. The low-temperature $H_2$ consumption band, which can be associated with reduction of maghemite to magnetite, corresponded to the same temperature range for Fe–Al–Cu (Fe/Cu = 10) and Fe–Al–Cu (Fe/Cu = 5) ($T_{max}$ = 270 and 261 °C, respectively), whereas the peak shifted to higher temperatures ($T_{max}$ = 296 °C) over Fe–Al–Cu (Fe/Cu = 2) sample. The shoulder peak at 230 °C in $H_2$ consumption trace of Fe–Al–Cu (Fe/Cu = 2) was assigned to reduction of CuO to metallic Cu, presence of which has been confirmed through XRD pattern of the reduced sample. The reduction peaks above 600 °C (in all samples) were assigned to over-reduction of active magnetite to WGS-inactive sub-oxides or to metallic Fe. These results were in agreement with those reported earlier [3] where aluminum and copper were suggested to facilitate magnetite formation, but did not affect reduction to metallic iron. The TPR studies indicated that optimum Cu content (Fe/Cu = 5) eased the reduction characteristic of iron oxide matrix (here, maghemite) to form active magnetite

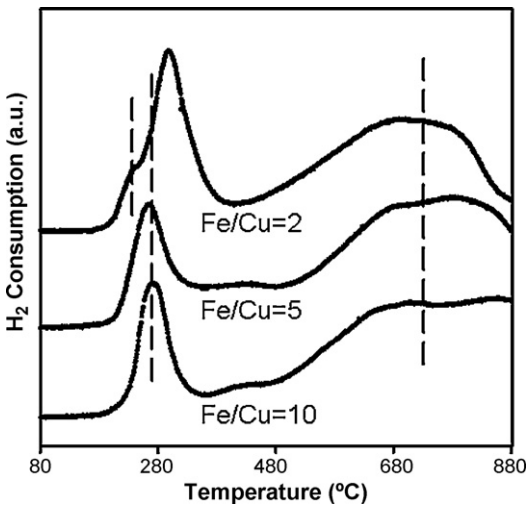


**Fig. 7.** Temperature-programmed reduction profiles of Fe–Al–Cu catalysts.

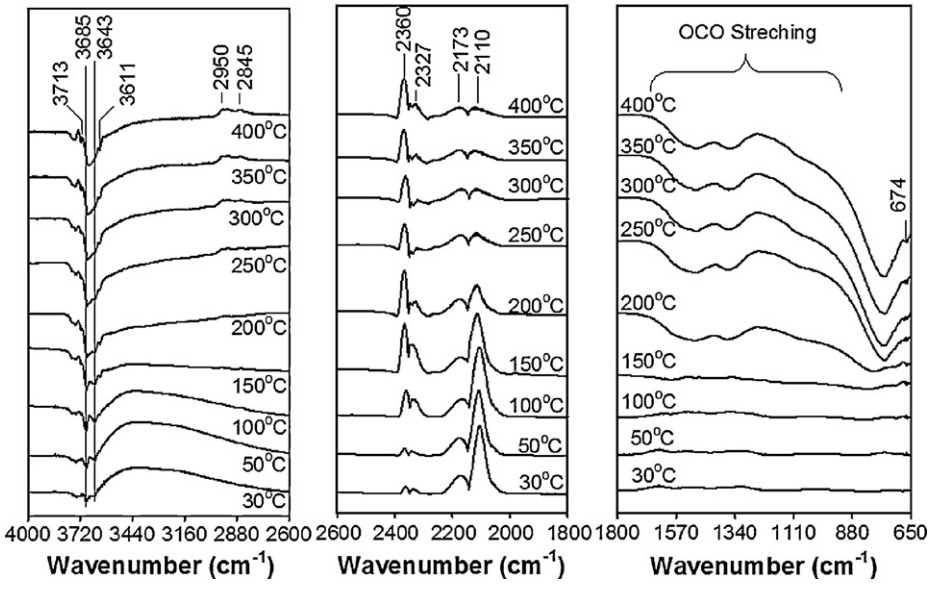


**Fig. 8.** DRIFTS study of CO interaction with Fe–Al–Cu (Fe/Cu = 5).

phase, whereas excess Cu content retarded the formation of the active phase during reduction. The segregation of a separate CuO phase was also demonstrated in these experiments.

### 3.2.5. *In situ* DRIFTS studies using CO

The interaction of CO with Fe–Al–Cu catalysts was investigated using *in situ* DRIFTS. Fig. 8 shows the DRIFTS spectra of CO adsorbed on the reduced Fe–Al–Cu sample in the temperature range of 30–400 °C. Bands in the range of 1000–1700 $cm^{-1}$ correspond to OCO symmetric as well as asymmetric stretching vibrations. However, carbonate and formate both contain OCO stretching and therefore it is difficult to distinguish between them. One possible way to is look for bands in the region 2800–3000 $cm^{-1}$ for C–H stretching [32] as formate species contain both OCO and C–H stretching. Fe–Al–Cu sample showed C–H stretching vibrations at 2845 and 2950 $cm^{-1}$, both could be due to bidentate formate or bidentate and bridging type formate species [33]. These C–H stretching features increased in intensity with increasing adsorption temperature. The bands at 2110 and 2173 $cm^{-1}$ assigned to weakly adsorbed CO and gas phase CO, respectively. The doublet of weakly adsorbed $CO_2$ was observed at 2327 and 2360 $cm^{-1}$ [23].

The bands in between 3500–3800 $cm^{-1}$ were characteristic of OH groups associated with the catalyst. The bands at 3643 and 3685 $cm^{-1}$ were assigned to Type II bridging OH group (geminal) [33,34] on the "reduced" Fe–Al–Cu catalyst. Jacobs et al. [33] reported that these Type II OH groups reacted with CO to form formate species for $Pt/CeO_2$ catalytic system. For Fe–Al–Cu, we observed that Type II OH groups diminished as temperature increased under the flow of CO while formate bands increased in intensity. Peaks at 3611 and 674 $cm^{-1}$ were the characteristic of hydroxyl vibrations associated with Cu [35]. The band at 3713 $cm^{-1}$ was assigned to Type I OH group (terminal) [33]. The OH stretching of adsorbed water was observed at 3400 $cm^{-1}$ [36] at lower temperatures, which disappeared above 100 °C.

While the presence of formate species may suggest an involvement as an intermediate in the reaction mechanism, it is also possible that they may be acting merely as spectators [37,38], and that the redox pathway is more likely to be the mechanism in operation in WGS reactions over these catalysts [19,23]. Temperature-programmed re-oxidation studies discussed in the next section also support this hypothesis. The catalyst re-oxidation studies suggest that a redox pathway may be the operative mechanism over these catalysts

### 3.2.6. Temperature-programmed re-oxidation

Re-oxidation of the catalyst surface constitutes an important step in water-gas shift reaction. Usually, surface oxygen vacancies are created through the oxidation of adsorbed CO and these vacancies act as sites for water adsorption to replenish surface oxygen [23,39,40]. Temperature-programmed re-oxidation experiments were performed following reduction of Fe–Al–Cu samples to study the re-oxidation kinetics of the catalysts and to determine the apparent activation energies of re-oxidation of the Fe–Al–Cu samples with Fe/Cu ratios of 2, 5 and 10.

The samples were reduced in 5%$H_2$/He at 300 °C and then, re-oxidized in 5%$O_2$/He while being heated at 10, 14 or 18 °C/min to 450 °C. The reduction temperature for these experiments was chosen in light of the TPR results discussed in Section 3.2.4, to enable reduction of γ-$Fe_2O_3$ to $Fe_3O_4$, but to prevent magnetite from being over-reduced. Fig. 9 shows oxidant consumption profiles during the temperature-programmed re-oxidation of reduced Fe–Al–Cu catalysts. At a heating rate of 10 °C/min, maximum oxidant consumption temperature corresponded to 201, 169 and 180 °C for Fe–Al–Cu (Fe/Cu = 2), Fe–Al–Cu (Fe/Cu = 5) and Fe–Al–Cu (Fe/Cu = 10), respectively. For Fe–Al–Cu (Fe/Cu = 2), the maximum oxidant consumption temperature shifted from 201 to 211 °C as the heating rate was increased from 10 to 18 °C/min (Fig. 9a). A shoulder in oxygen consumption profile was also resolved at 135 °C. In line with the $H_2$-TPR results, this $O_2$ consumption feature could be associated with oxidation of metallic copper species on the surface which have not been incorporated to the iron oxide matrix. Over Fe–Al–Cu (Fe/Cu = 5) and Fe–Al–Cu (Fe/Cu = 10), the temperature for maximum oxidant consumption shifted from 168 to 200 °C and from 180 to 188 °C, respectively. The oxidant consumption traces were composed of a single component, therefore no evidence for the formation of metallic copper domains through diffusion of copper species from the iron oxide matrix to the surface during reduction was present over these samples.

In a plot of oxidant consumption as a function of temperature, the deflection point gives the temperature ($T_m$) at which the oxidant consumption rate is a maximum. The temperature of maximum oxidant consumption rate shifted to higher temperatures as the heating rate ($\Phi$) was increased and a plot of $1/T_m$ versus $\ln(\Phi/T_m^2)$ was used to determine the activation energy for the re-oxidation process. In line with the above discussion on the selection of the reduction temperature, the apparent activation energies for re-oxidation calculated through Arrhenius plots were linked to re-oxidation of $Fe_3O_4$. The inset to Fig. 9a shows the plot of $1/T_m$ versus $\ln(\Phi/T_m^2)$ which gives a straight line with a slope of −12.48 that corresponded to activation energy of 103.76 kJ/mol for re-oxidation of Fe–Al–Cu (Fe/Cu = 2). Similarly, the activation energies for re-oxidation were calculated as 25 and 115 kJ/mol for Fe–Al–Cu (Fe/Cu = 5) and Fe–Al–Cu (Fe/Cu = 10), respectively. Based on the activation energies, the re-oxidation of Fe–Al–Cu (Fe/Cu = 2) and Fe–Al–Cu (Fe/Cu = 10) is expected to take place at a much slower rate than Fe–Al–Cu (Fe/Cu = 5).

Iron oxide-chromium catalysts have been shown to have apparent WGS activation energies in the order of 110–130 kJ/mol [5,41,42]. Hutchings and co-workers [5,21] further showed that incorporation of copper into the Fe–Cr system reduced the appar-

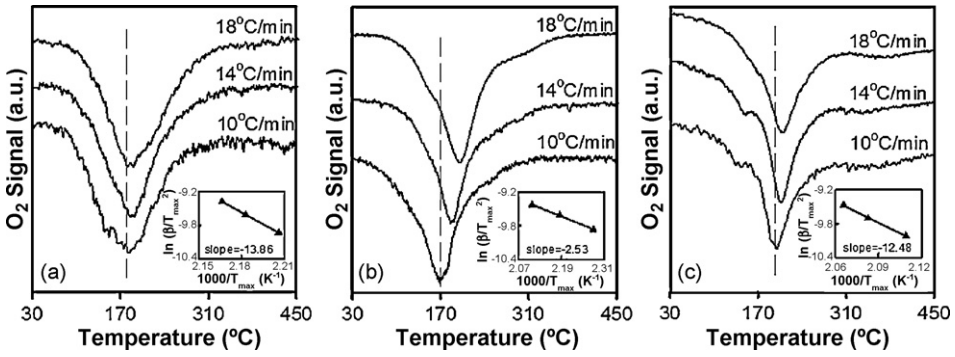


**Fig. 9.** Temperature-programmed re-oxidation of reduced Fe–Al–Cu samples at different ramp rates: (a) Fe/Cu = 10, (b) Fe/Cu = 5 and (c) Fe/Cu = 2. Insets show determination of activation energies of re-oxidation using the Kissinger method.

ent activation energy for WGS reaction and reported activation energies in the order of 80 kJ/mol for this system. The apparent activation energies of re-oxidation of Fe–Al–Cu samples showed that while the re-oxidation of Fe–Al–Cu (Fe/Cu = 2) and Fe–Al–Cu (Fe/Cu = 10) samples proceed at a rate comparable to (if not slower than) the reduction of the surface during oxidation of adsorbed CO with surface oxygen, the re-oxidation of Fe–Al–Cu (Fe/Cu = 5) proceeded at a much faster rate than the reduction. Therefore, WGS reaction over the Fe–Al–Cu (Fe/Cu = 5) sample would solely be controlled by reduction kinetics of the surface whereas for the Fe–Al–Cu (Fe/Cu = 2) and Fe–Al–Cu (Fe/Cu = 10) availability of surface oxygen for CO oxidation would be a rate determining factor. These results are consistent with the reaction experiments which showed a much more pronounced improvement over the Fe–Al–Cu (Fe/Cu = 2) and Fe–Al–Cu (Fe/Cu = 10) when steam-to-CO ratio was doubled. The catalysts which had the higher activation energy barriers for re-oxidation benefited more from the increased water concentration than the catalyst which had a lower activation energy for re-oxidation with water. Although the presence of formate species have been observed in the DRIFT spectra which does not allow us to rule out the formate mechanism during WGS reaction, the catalyst re-oxidation studies suggest that a redox pathway may be the operative mechanism over these catalysts.

## 4. Conclusions

Gelation agent-assisted one-pot sol–gel technique was used for preparation of Fe-based WGS catalysts. Propylene oxide and citric acid were investigated as the gelation agents. Propylene oxide emerged as a more suitable gelation agent than citric acid. The effect of Cu-loading study showed that Fe–Al–Cu (Fe/Cu = 5) was the optimum Cu loading and the excess amount of copper in Fe–Al–Cu (Fe/Cu = 2) caused significant decrease in the WGS activity. With increasing copper content, segregation of a copper-containing phase, which is more prone to reduction under reaction conditions, was observed through XRD and TPR.

The apparent activation energies of re-oxidation of Fe–Al–Cu (Fe/Cu = 10) and Fe–Al–Cu (Fe/Cu = 2) were found to be much higher than Fe–Al–Cu (Fe/Cu = 5). The apparent activation energies of re-oxidation of the Fe–Al–Cu catalysts suggested that WGS reaction over Fe–Al–Cu (Fe/Cu = 5) was controlled by the rate of reduction of the surface through oxygen removal by CO, whereas for Fe–Al–Cu (Fe/Cu = 10) and Fe–Al–Cu (Fe/Cu = 2) reduction and re-oxidation of the surface would proceed at comparable rates. Increasing water concentration in the feed showed a more pronounced improvement in CO conversion over the catalysts with high activation energy barriers for re-oxidation.

## Acknowledgements

The authors acknowledge the contribution of Dr. Lingzhi Zhang to the initial phases of this project. Financial support provided by the Ohio Coal Development Office and by the U.S. Department of Energy through the grant DE-FG36-05GO15033 is gratefully acknowledged.

The authors also acknowledge NSF support for the acquisition of the XPS system under NSF-DMR grant #0114098.

## References

[1] A.O. Souza, M.C. Rangel, React. Kinet. Catal. L79 (2003) 175–180.
[2] J. Souza, M. Rangel, React. Kinet. Catal. L83 (2004) 93–98.
[3] G.C. Araújo, M.C. Rangel, Catal. Today 62 (2000) 201–207.
[4] M. Sohrabi, A. Irandoukht, React. Kinet. Catal. L80 (2003) 303–309.
[5] C. Rhodes, G.J. Hutchings, Phys. Chem. Chem. Phys. 5 (2003) 2719–2723.
[6] R.J. Gorte, S. Zhao, Catal. Today 104 (2005).
[7] D.L. Trimm, Z.I. Onsan, Catal. Rev. Sci. Eng. 43 (2001).
[8] E.B. Quadro, M.L.R. Dias, A. Maria, M. Amorim, M.C. Rangel, J. Braz. Chem. Res. 10 (1999) 51–59.
[9] J.L. Rangel Costa, G.S. Marchetti, M.C. Rangel, Catal. Today 77 (2002) 205–213.
[10] Q. Liu, W. Ma, R. He, Z. Mu, Catal. Today 106 (2005) 52–56.
[11] M. Zayat, D. Levy, Chem. Mater. 12 (2000) 2763–2769.
[12] H. Cui, M. Zayat, D. Levy, J. Sol–Gel Sci. Technol. 35 (2005) 175–181.
[13] A.E. Gash, T.M. Tillotson, J. Joe, H. Satcher, J.F. Poco, L.W. Hrubesh, R.L. Simpson, Chem. Mater. 13 (2001) 999–1007.
[14] W. Dong, C. Zhu, J. Mater. Chem. 12 (2002) 1676–1683.
[15] M. Anilkumar, R. Pasricha, V. Ravi, Ceram. Int. 31 (2005) 889–891.
[16] D. Segal, J. Mater. Chem. 7 (1997) 1297.
[17] S.R. Dhage, S.P. Gaikwad, P. Muthukumar, V. Ravi, Mater. Lett. 58 (2004) 2704–2706.
[18] S.R. Dhage, R. Parsicha, V. Ravi, Mater. Res. Bull. 38 (2003) 1623–1628.
[19] L. Zhang, X. Wang, J.-M.M. Millet, P.H. Matter, U.S. Ozkan, Appl. Catal. A-Gen. 351 (2008) 1–8.
[20] L. Zhang, J.-M.M. Millet, U.S. Ozkan, Appl. Catal. A-Gen. 357 (2009) 66–72.
[21] C. Rhodes, B.P. Williams, F. King, G.J. Hutchings, Catal. Commun. 3 (2002) 381–384.
[22] H.E. Kissinger, Anal. Chem. 29 (1957) 1702–1706.
[23] S. Natesakhawat, X. Wang, L. Zhang, U.S. Ozkan, J. Mol. Catal. A 260 (2006) 82–94.
[24] X. Liang, X. Wang, J. Zhuang, Y. Chen, D. Wang, Y. Li, Adv. Funct. Mater. 16 (2006) 1805.
[25] M.L. Kundu, A.C. Sengupta, G.C. Maiti, J. Catal. 112 (1988) 375.
[26] M.A. Edwards, D.M. Whittle, C. Rhodes, A.M. Ward, D. Rohan, M.D. Shannon, G.J. Hutchings, C.J. Kiely, Phys. Chem. Chem. Phys. 4 (2002) 3902–3908.
[27] J.F. Moulder, W.F. Stickle, P.E. Sobol, K.D. Bomben, Handbook of X-ray Photoelectron Spectroscopy, Perkin Elmer Corporation, Physical Electronics Division, Eden Prairie, 1992.
[28] D.C. Frost, A. Ishitani, C.A. McDowell, Mol. Phys. 24 (1972) 861–877.
[29] D.E. Mencer, M.A. Hossain, R. Schennach, T. Grady, H. McWhinney, J.A.G. Gomes, M. Kesmez, J.R. Pargad, T.L. Barre, D.L. Cocke, Vacuum 77 (2004) 27–35.
[30] C.-K. Wu, M. Yin, S. O'Brien, J.T. Koberstein, Chem. Mater. 18 (2006) 6054–6058.
[31] N.S. McIntyre, D.G. Zetaruk, Anal. Chem. 49 (1975) 1521–1529.
[32] G. Jacobs, P.M. Patterson, L. Williams, E. Chenu, D. Sparks, G. Thomas, B.H. Davis, Appl. Catal. A-Gen. 262 (2004) 177–187.
[33] G. Jacobs, U. Graham, E. Chenu, P.M. Patterson, A. Dozier, B.H. Davis, J. Catal. 229 (2005) 499–512.
[34] G. Jacobs, G.M. Patterson, U.M. Graham, D.E. Sparks, B.H. Davis, Appl. Catal. A-Gen. 269 (2004) 63–73.
[35] C.J.G. van der Grift, J.W. Geu, M.J. Kappers, J.H. van der Maas, Catal. Lett. 3 (1989) 159–168.
[36] G. Smit, N. Strukan, M. Craje, K. Lazar, J. Mol. Catal. A 252 (2006) 163–170.
[37] C. Rhodes, G.J. Hutchings, A.M. Ward, Catal. Today 23 (1995) 43–58.
[38] R.M. Van Natter, J.S. Coleman, C.R.F. Lund, J. Mol. Catal. A 292 (2008) 76–82.
[39] J.E. Kubsh, J.A. Dumesic, AIChE J. 28 (1982) 793.
[40] C.R. Lund, J.E. Kubsh, J.A. Dumesic, in: R.K. Graselli, J.F. Bradzil (Eds.), Solid State Chemistry in Catalysis, American Chemical Society, Washington, DC, 1985, p. 19.
[41] G.C. Chinchen, J.E. Kubsh, J.A. Dumesic, Appl. Catal. 12 (1984) 97–103.
[42] R.L. Keiski, O. Desponds, Y.F. Chang, G.A. Somorjai, Appl. Catal. A 101 (1993) 317–338.